



Prototype of interferometric absolute motion sensor

C. Collette^{a,*}, F. Nassif^a, J. Amar^a, C. Depouhon^a, S.-P. Gorza^b

^a Université Libre de Bruxelles, BEAMS Department, F.D. Roosevelt 50, B-1050 Brussels, Belgium

^b Université Libre de Bruxelles, OPERA Department, F.D. Roosevelt 50, B-1050 Brussels, Belgium

ARTICLE INFO

Article history:

Received 4 November 2014

Received in revised form 20 January 2015

Accepted 20 January 2015

Available online 29 January 2015

Keywords:

Inertial sensor
Accelerometer
Seismometer
Geophone

ABSTRACT

For many applications, there is an increasing demand for low cost, high resolution inertial sensors, which are capable of operating in harsh environments. Based on recent developments in optical seismometry, this paper presents a new small interferometric inertial sensor with a resolution of $3 \text{ pm}/\sqrt{\text{Hz}}$ above 4 Hz. Compared to most state-of-the-art devices, this prototype does not contain any coil, which offers several important advantages: (i) when it is used for active control, it magnifies the control performances around the sensor resonance; (ii) it decreases the thermal noise in the suspension (Brownian motion); (iii) it is compatible with magnetic environments (like particle collider); (iv) as the interference fringes sweep continuously across the detector, it allows a real time calibration of the parameters, and thus the calibration can be continuous monitored and updated.

© 2015 Elsevier B.V. All rights reserved.

1. Introduction

Inertial sensors have been used for more than a century mainly to answer the needs of seismology, the science which studies the propagation of waves through the Earth. Depending on the frequency range of interest, three types of sensors are commonly used to measure seismic vibrations [1]: seismic accelerometers, geophones and broadband seismometers. A comparison of these inertial sensors can be found in [2].

For more than 30 years, seismometers have reached sufficient resolution and dynamic range to capture seismic signals at most location of the Earth surface in a broad frequency range extending typically from 1 min to 100 Hz (see e.g. [3–6]). However, there is still a continuous demand for high-end instruments, more efficient and better adapted to some specific applications. In this respect, recent developments in optical technologies offer interesting perspectives for novel inertial sensors. In the oil/gas and mining industry for instance, inertial sensors capable of operating in harsh environments (e.g. down-holes, boreholes) are needed, and optical seismometers without electronics and insensitive to temperature and high pressure [7–10] have been developed. In the field of security, miniature autonomous optical inertial sensors have been tested for the detection of detonation arising from nuclear tests conducted by countries engaged in nuclear proliferation [11–13].

Besides seismology and the aforementioned applications, there is also a demand for inertial sensors for precision engineering and scientific experiments requiring a very stable environment [14]. Typical applications are: (i) Tests and validation of space equipments on vibration-free space simulator. (ii) Isolation of lithography machines in the semiconductor industry. (iii) Reduction of vibrations of atomic force microscopes (support and sample) for increasing their resolution. (iv) Stabilization and isolation of large instruments dedicated to extreme experimental physics, like gravitational wave interferometric detectors or future particle colliders. In these systems the immunity to environmental disturbances is obtained by actively cancelling the structural vibration measured by inertial sensors [15].

A few other prototypes of optical inertial sensors and seismometers have been developed and reported in the literature. They are based on Fabry-Perot interferometer [22], fiber interferometer [19–21], triangulation system [23], fiber Bragg grating [24,25], optical encoder [26] or grating sensor [27]. More recently, optical accelerometers have been proposed for measuring the mechanical vibration of gravitational wave detectors [16–18].

However, to the best of the authors' knowledge, there is no commercial seismometer capable of fulfilling the requirements for applications in advanced active vibration isolation systems, i.e. small, sub-nanometer resolution at low frequency, and compatible with a magnetic environment. In this paper, we present a non-magnetic Optical inertial SEnsor (NOSE), which is based on a horizontal pendulum and a Michelson interferometer. It is small,

* Corresponding author. Tel.: +32 26502840.

E-mail address: christophe.collette@ulb.ac.be (C. Collette).

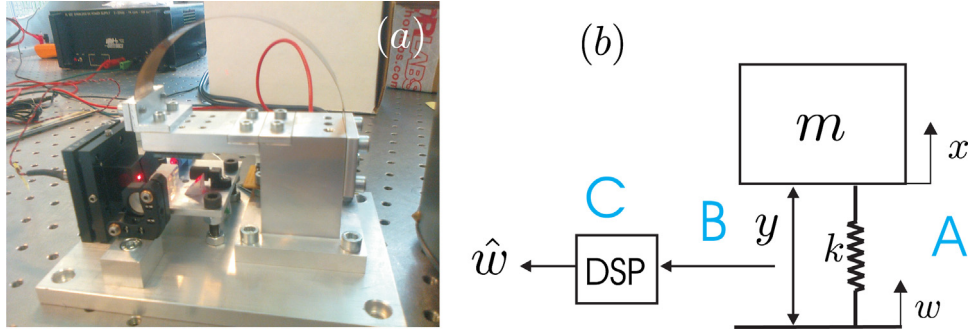


Fig. 1. Picture (a) and schematic (b) of the prototype of the interferometric inertial sensor NOSE. (A) Single degree of freedom oscillator, (B) interferometric displacement sensor and (C) acquisition processing unit.

passive, and measures seismic motion in the vertical direction.¹ We will show that, besides the compatibility with magnetic environment, the absence of coil offers also several advantages.

The paper is organized as follows: The new sensor is presented in Section 2. Section 3 contains experimental validations, and Section 4 draws the conclusions and directions for improvements.

2. Description of the optical inertial sensor

The sensor is composed of three main parts (see Fig. 1): A single degree of freedom (d.o.f) oscillator (A), an interferometric displacement sensor (B), and an acquisition processing unit (C). Each of the three parts are detailed in the following sections.

2.1. Mechanics

The mechanical part consists of a horizontal pendulum, connected to a rigid frame through a flexural joint, made of CuBe alloy. A leaf spring, made of the same alloy, is used to adjust the equilibrium position of the inertial mass and compensate for gravity. The oscillator is characterized by an inertial mass $m = 0.055 \text{ kg}$, a principal resonance frequency $\omega_0 = 6 * 2\pi \text{ rad/s}$ (tunable) and spurious resonances above 100 Hz.

Usually, and most specifically for geophones, a high damping of the inertial mass, i.e. a small Q factor, is imposed in order to increase the bandwidth of the sensor and reduce its sensitivity to miscalibration. A critical damping is obtained by connecting a resistor to the sensing coil. On the contrary, our inertial sensor is characterized by a high Q factor (around 60) because it does not contain any loaded coil. A first advantage of the coil-free configuration is that the sensor is compatible with magnetic environments like encountered in proximity to particle colliders. A second advantage is that the high Q decreases the thermal noise in the suspension (Brownian motion) defined as [28]:

$$B(f) = \frac{\sqrt{4k_B T \omega_0 m / Q}}{m(2\pi f)^2} \simeq 10^{-11} f^{-2} [m/\sqrt{\text{Hz}}] \quad (1)$$

where k_B is the Boltzmann constant, $T = 300 \text{ K}$ is the temperature and ω_0 is the angular resonance frequency.

When the inertial sensor is used for active vibration isolation, the high Q offers a third advantage because it magnifies the control performance around the sensor resonance. As an example, consider the single d.o.f. isolator shown in Fig. 2(a) where a sensitive equipment (m) mounted on an active suspension is represented. The motion x of the equipment is measured with

an inertial sensor. Then, the signal is filtered by a filter $H(s)$, used to generate a feedback force f . Fig. 2(b) shows a typical transmissibility (x/w) of the suspension when the control is turned off (solid line), and turned on for two sensors: a geophone critically damped (dotted line) and NOSE (dashed line). The same controller $H(s)$ has been used for both sensors. The curves have been obtained with a numerical model of the isolator, and the following numerical values of the parameters: $m = 100 \text{ kg}$, $k = 1.6 \text{ MN/m}$, $c = 1200 \text{ Ns/m}$. The figure shows that, for both sensors, the transmissibility has been reduced by the feedback operation in a large bandwidth, extending from a fraction of the geophone corner frequency to a multiple of the resonance of the equipment.

However, for NOSE, the strong mechanical amplification at the resonance improves significantly the isolation in a frequency range around this resonance, while using the same crossover frequencies for both sensors. Such feature can be particularly interesting to cancel narrow band excitations. Moreover, as the photo-diodes signals amplitude remains bounded (see Section 2.3), the peak of performance is not limited by the classical trade-off between resolution and dynamic range.

On the other hand, when the sensor is not used in a feedback loop, the low damping of the inertial mass becomes a disadvantage because it reduces the bandwidth and because large oscillations of the inertial mass are superimposed to the useful signal. Still, the absence of coil remains interesting for the compatibility with magnetic environments.

2.2. Interferometric sensor

In order to measure the relative displacement between the inertial mass and the support, we have developed a sensor based on a Michelson interferometer, adapted to enable the measurement of both quadratures of the signals as in [7,29]. The optical scheme is shown in Fig. 3.

The laser source is a He-Ne laser with a wavelength of 632.8 nm. The input beam, linearly polarized at 45°, is first split in two orthogonal beams by means of a 50/50 non polarizing beam splitter (BS). Each beam is then reflected on the mirrors M_1 or M_2 . M_1 is fixed on the inertial mass and M_2 is mounted on a miniature two d.o.f. tilt stage to enable the alignment of the interferometer. Additionally, the arm d_2 contains a $\lambda/8$ waveplate to generate a circularly polarized beam (it is in an elliptical polarization after 1 pass, and a circular polarization after double-passing the wave plate). The two beams are recombined in the beams splitter (BS). The vertically and the horizontally polarized components of the recombined beam are then separated by a polarizing beam splitter (PBS). The intensity in the two beams are finally measured by means of two photodiodes. The laser source is mounted on a four d.o.f. stage (two translations and two rotations) to adjust the position and the angle of the beams

¹ In principle, the sensor is also capable to measure seismic motion in the horizontal direction. However, this feature has not been investigated.

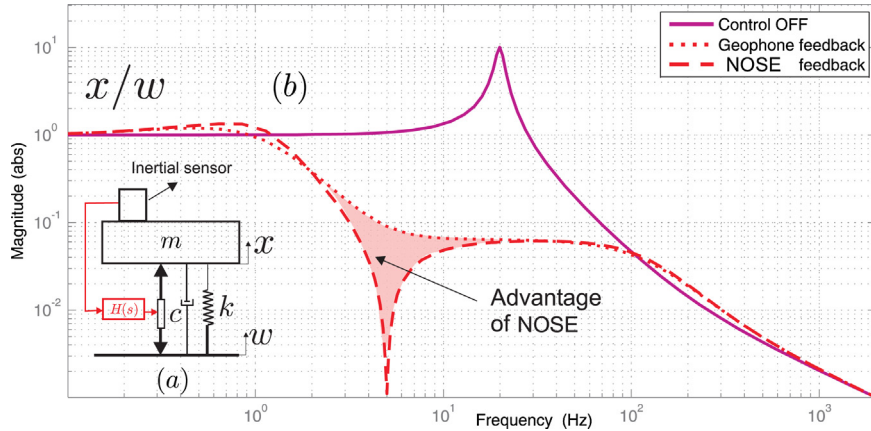


Fig. 2. (a) Principle of active vibration isolator using inertial sensor; (b) simulated transmissibility (x/w) of the numerical model of the isolator shown in (a) when the controller is turned off, turned on using a commercial geophone, and turned on using a low damped inertial sensor like NOSE.

on the photodiodes. The length of the two arms (d_1 and d_2) are similar to minimize the impact of the laser frequency noise on the measurements [30]. Note that the He–Ne laser can be replaced by a pigtailed laser diode with a polarization-maintaining optical fiber [8] and a fiber collimator.

2.3. Acquisition and processing

The two photodiode signals ($PD1$ and $PD2$) have the general form:

$$\begin{cases} PD1 = a_1 + b_1 \cos(\varphi_0 + \varphi) \\ PD2 = a_2 + b_2 \sin(\varphi) \end{cases} \quad (2)$$

where the amplitudes a_1 , a_2 , b_1 , b_2 depend on the actual setup (losses and beams alignment), and φ is the phase proportional to the relative displacement Δx of the mirror M_2

$$\varphi = \frac{4\pi}{\lambda} \Delta x, \quad (3)$$

λ being the wavelength of the laser source; and where φ_0 takes into account possible deviation of the phase delay from $\pi/4$ in the octaedric waveplate. Fig. 4 shows a typical example of an experimental Lissajous figure (blue curve) obtained when the first photodiode signal ($PD1$) is plotted against the other ($PD2$). Note that, in this example, the fringe visibility is not maximum.

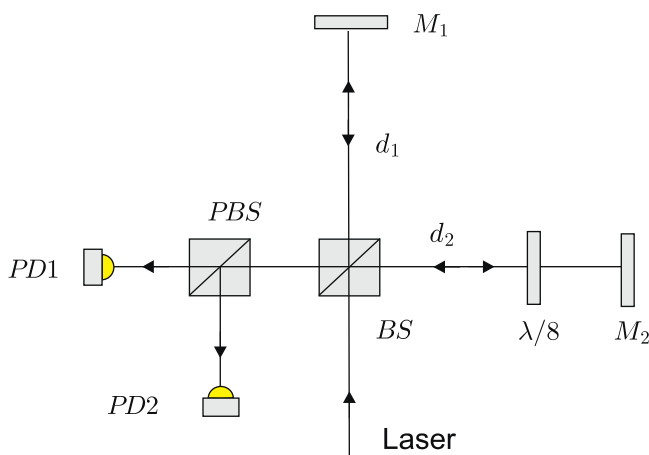


Fig. 3. Optical scheme of the interferometer used in NOSE.
Adapted from [8].

Several methods are reported in the literature to demodulate the signals and extract the phase. In [32], the sine and cosine components are normalized, using the signal from a third photodiode. In some other techniques, the signals are derived and recombined to extract the phase. However, it has been observed that these techniques are quite noise sensitive, resulting in a decrease of the signal to noise ratio. In another technique described in [31,33], the parameters of the Lissajous figure are first calculated to transform the ellipse in a unit circle centered on the origin (see in Fig. 4, green curve) from which the phase can readily be extracted. This technique has been proven to be robust and was then used to extract the displacement parameter from the recorded data.

In operating condition, the mass, subjected to the excitation from the ground motion, oscillates continuously at its resonance frequency, with an amplitude proportional to the Q factor of the oscillator times the amplitude of the ground motion at the sensor location. A high Q factor, as for NOSE, leads to a large motion of the inertial mass and results in a continuous sweeping of the interference fringes across the detector. This is a fourth advantage of a high Q factor, because it allows a real time estimation of the Lissajous figure parameters, and thus an unbiased demodulation of the signals. Another asset of this technology is that, since the amplitude of the photodiode signals is bounded in an interferometric displacement

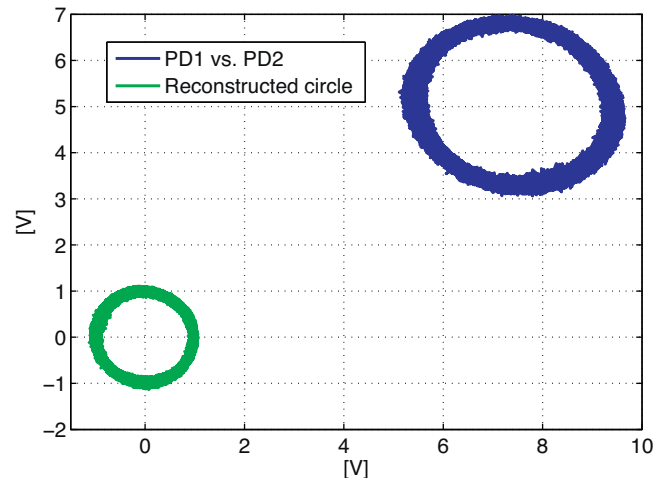


Fig. 4. Example of experimental Lissajous figure (blue curve) obtained when the first photodiode signal ($PD1$) is plotted against the other ($PD2$). Unit circle centered on the origin (green) calculated using the parameters of the ellipse and an algorithm described in [31]. (For interpretation of the references to color in this figure legend, the reader is referred to the web version of the article.)

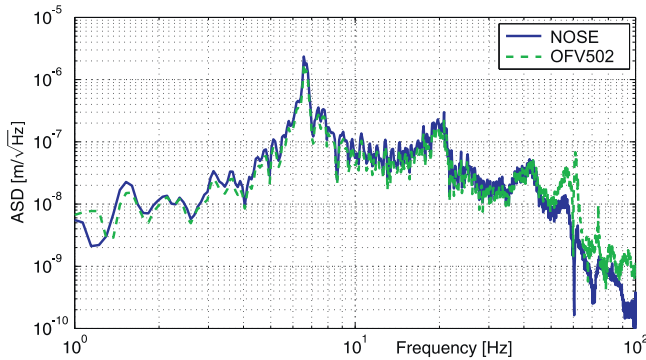


Fig. 5. Experimental amplitude spectrum of the Polytec OFV502 (dashed green line) compared to our prototype of inertial sensor NOSE (solid blue line). (For interpretation of the references to color in this figure legend, the reader is referred to the web version of the article.)

sensor, an equivalent of 30 bit resolution can be obtained with only a 16 bits A/D converter.

The next section presents the results of three experiments: a validation of the interferometric displacement sensor (NOSE), an identification of the different sources of noise in the signal, and an experimental validation of NOSE by comparison with a commercial seismometer.

3. Experiments

3.1. Assessment of the interferometer

As a first step, we have made an experiment to confirm that the displacement measured with our interferometer prototype corresponds to the actual displacement of the inertial mass. To this end, the output signal of NOSE was compared to the measured displacement of the inertial mass by a commercial interferometer (Polytec OFV502). The lower side of the inertial mass was pointed by our interferometer, while the upper side was pointed by the commercial sensor. The amplitude spectrum of the two measured signals are plotted in Fig. 5.

It can be seen that both spectra are nearly identical, from DC to approximately 50 Hz. The transfer function between the Polytec OFV502 and our interferometer is shown in Fig. 6. A very good agreement between the two sensors is obtained in the frequency range 0.1–50 Hz. The scale factor of 0.8 has not been investigated. The peaks in the transfer function around 60 Hz and above have been identified to correlate with resonances of the Polytec OFV502 head holder.

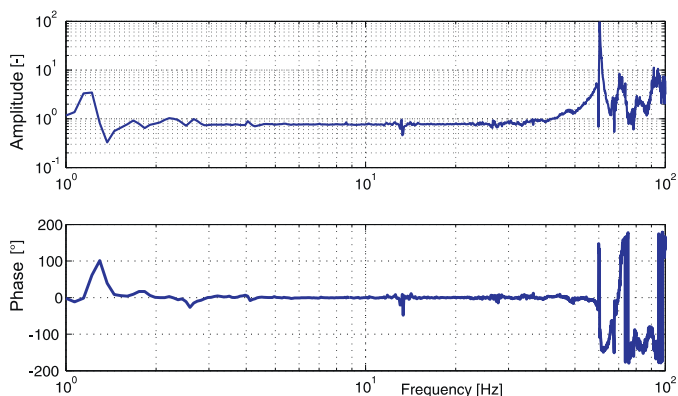


Fig. 6. Experimental amplitude and phase of the transfer function between the Polytec OFV502 and our prototype of inertial sensor, pointing the upper and lower side of the inertial mass, respectively.

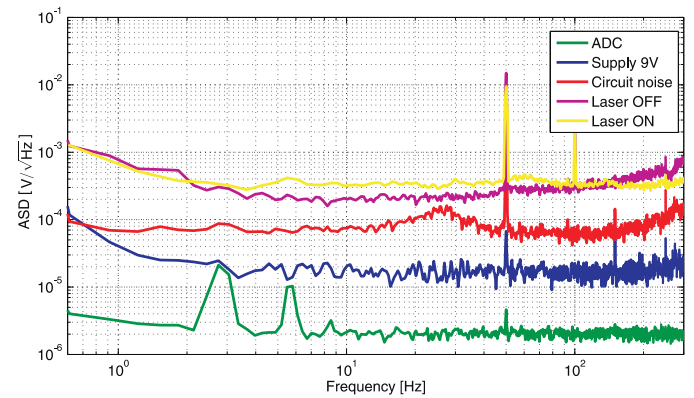


Fig. 7. Experimental noise budgeting of the interferometer.

3.2. Noise budgeting

An expected feature of the NOSE sensor is its ability to measure low frequency vibrations with a good resolution. In order to identify the various sources of noise, which are the factors limiting the sensor resolution, we have blocked the inertial mass and recorded the photodiode signals in the configurations listed below (the corresponding experimental amplitude spectra are plotted in Fig. 7):

- Cable unplugged from the recorder (ADC noise).
- Voltage source alone, when it supplies 9 V (Source noise).
- The voltage source supplies 9 V to the circuit, but the photodiode is not connected (Circuit noise)
- The voltage source supplies 9 V to the circuit, the photodiode is connected, but the laser switched off (Laser OFF)
- The voltage source supplies 9 V to the circuit, the photodiode is connected, and the laser switched on (Laser ON)

In our experiment, the sampling frequency is 20 kHz. Fig. 7 shows that the resolution is limited by a constant voltage noise above 2 Hz, and by a 1/f current noise below 2 Hz coming from the laser optical power noise [30].

The sharp peaks at 50 Hz and multiples of 50 Hz are related to the electrical supply network. These peaks can be removed by using an electromagnetic shielding of the sensor, and by using batteries to supply the operational amplifiers.

Fig. 8 shows the experimental amplitude spectrum of the interferometer noise (blue dashed-dotted line), expressed in physical units of $[\text{m}/\sqrt{\text{Hz}}]$. It has been obtained in two steps. In the first step, we manually slightly moved one mirror in order to obtain the

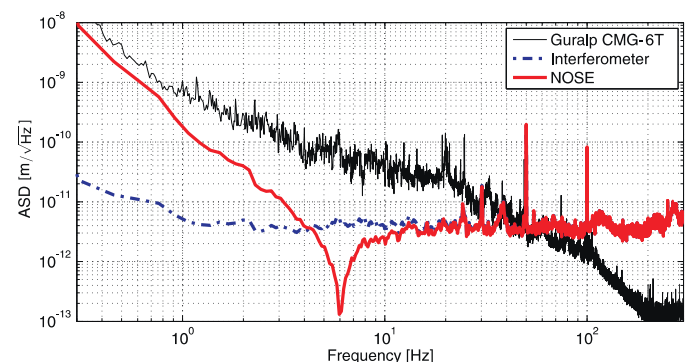


Fig. 8. Comparison of sensor experimental resolution: Guralp CMG-6T (black line, obtained from two sensors side by side placed in a quiet environment); resolution of our NOSE prototype, measured by blocking the inertial mass; estimated resolution of NOSE (red line). (For interpretation of the references to color in this figure legend, the reader is referred to the web version of the article.)

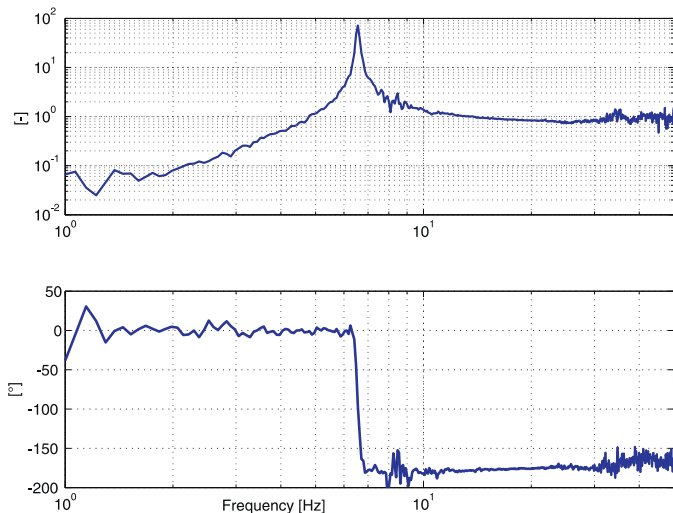


Fig. 9. Experimental amplitude and phase of the transfer function between the signal from a commercial Guralp CMG-6T calibrated in displacement units and our prototype NOSE.

parameters of the Lissajous figure for the calibration. In a second step, we have recorded the signal without disturbing the interferometer, and used the parameters from the first step to express the photodiode signals as sensor noise in displacement units. It results in a resolution of $3 \text{ pm}/\sqrt{\text{Hz}}$ above 1 Hz, and $20 \text{ pm}/\sqrt{\text{Hz}}$ above 0.3 Hz.

3.3. Assessment of the inertial sensor

In order to confirm that our sensor measures properly seismic motion, we made a third experiment where the output signal of our prototype was compared to the readout of a commercial seismometer (Guralp CMG-6T), located beside our sensor. Fig. 9 shows the experimental transfer function between the sensors (calibrated in displacement units), which corresponds to the sensitivity curve of NOSE, because the CMG-6T has a constant sensitivity from 30 s to 100 Hz.

Dividing the interferometer resolution (Fig. 8) by the sensor transfer function (Fig. 9) gives the estimation of the NOSE resolution, also shown in Fig. 8 (red curve). The resolution of the Guralp CMG-6T (measured in a quiet environment with two sensors side by side) is also shown in the same figure for comparison. Below 50 Hz, NOSE resolution overpasses GMG-6T, by up to a factor 100 around 6 Hz, because of the mechanical resonance. At that frequency, NOSE resolution peaks at $0.1 \text{ pm}/\sqrt{\text{Hz}}$.

4. Conclusion and future work

We have presented a new small, low cost, non-magnetic optical inertial sensor, called NOSE. Compared to most state-of-the-art commercial inertial sensors, this prototype does not contain any coil, resulting in a huge amplification of the response at the sensor resonance. We have shown that, when combined to an interferometric sensor, this feature offers four important advantages: (i) when used for active control, it magnifies the control performance around the sensor resonance; (ii) the suspension has a low thermal noise, (iii) it is compatible with magnetic environments (like encountered in particle collider); (iv) it allows a real time calibration of the parameters, and thus an unbiased demodulation of the signal tanks to the continuous sweeping of the fringes across the detectors. Using low cost components, we have demonstrated a resolution of $3 \text{ pm}/\sqrt{\text{Hz}}$ above 4 Hz. The prototype has been validated

experimentally by comparison with state-of-the-art commercial inertial sensors.

In the future, we plan to measure the sensor sensitivity to magnetic field and increase the performance by reducing the photo-diode dark noise, using a stabilized source, optimizing the mechanical design (for a better integration and smaller size), and by automatizing the signal processing.

Acknowledgments

The authors gratefully acknowledge the Brussels Capital Region for funding and supporting this research. We also warmly acknowledge Prof. Iulian Romanescu for his help to construct the mechanical parts. Many thanks to Stef Janssens and Kurt Artoos for their collaboration, and for lending the Guralp seismometers, and to our colleagues at the LIGO Lab of the Massachusetts Institute of Technology for numerous inspiring discussions on interferometric inertial sensors. This document has been assigned LIGO Laboratory document number LIGO-P1400115.

References

- [1] E. Wienlandt, Seismometry, in: W.H.K. Lee, H. Kanamori, P.C. Jennings, C. Kisslinger (Eds.), International Handbook of Earthquake and Engineering Seismology, Part A, Academic Press, Amsterdam, 2002, pp. 283–304.
- [2] C. Collette, S. Janssens, P. Fernandez-Carmona, K. Artoos, M. Guinchard, C. Hauviller, A. Preumont, Review: inertial sensors for low-frequency seismic vibration measurement, Bull. Seismol. Soc. Am. 102 (4) (2012) 1289–1300.
- [3] H.E. Sheffield, An electronic vertical long-period seismometer, IEEE Trans. Inst. Meas. 13 (1964) 2–7.
- [4] C. Teupser, A. Plesinger, Design of feedback-controlled wide-band seismographs with respect to undesired side-effects, Phys. Earth Planet. Inter. 18 (1979) 58–63.
- [5] M.J. Usher, R.F. Burch, C. Guralp, Wide-band feedback seismometers, Phys. Earth Planet. Inter. 18 (1979) 38–50.
- [6] E. Wielandt, G. Sterkeisen, The leaf spring seismometer: design and performance, Bull. Seismol. Soc. Am. 72 (1982).
- [7] M. Zumberge, J. Berger, J. Otero, E. Wielandt, An optical seismometer without force feedback, Bull. Seismol. Soc. Am. 100 (2) (2010) 598–605.
- [8] J. Otero, Development and Characterization of an Observatory-class, Broadband, Non-Fedback, Leaf-Spring Interferometric Seismometer (PhD thesis), University of California, San Diego, 2009.
- [9] M. Zumberge, J. Berger, E. Wielandt, Optical seismometer, US patent 2012/0247213 A1, 2012.
- [10] USSI, <http://www.usssensorsystems.com/USSI-Geophone-brochure.pdf>
- [11] D. Carr, G. Bogart, S. Goodman, P. Baldwin, D. Robinson, A laser interferometric miniature seismometer, in: Monitoring Research Review: Ground-Based Nuclear Explosion Monitoring Technologies, 2008.
- [12] D. Carr, P. Baldwin, S. Knapp-Kleinsorge, H. Milburn, D. Robinson, A Laser Interferometric Miniature Seismometer, 2010, pp. 268.
- [13] D. Carr, P. Baldwin, S. Knapp-Kleinsorge, H. Milburn, D. Robinson, A laser interferometric miniature seismometer, in: Monitoring Research Review: Ground-Based Nuclear Explosion Monitoring Technologies, 2011.
- [14] P. Shore, C. Cunningham, D. DeBra, C. Evans, J. Hough, R. Gilmozzi, H. Kunzmann, P. Morantz, X. Tonnellier, Precision engineering for astronomy and gravity science, CIRP Ann. Manuf. Technol. 59 (2010) 694–716.
- [15] C. Collette, S. Janssens, K. Artoos, Review of active vibration isolation strategies, Recent Patents Mech. Eng. 4 (2011) 212–219.
- [16] F. Acerne, G. Giordano, R. Romano, R. De Rosa, F. Barone, Mechanical monolithic horizontal sensor for low frequency seismic noise measurement, Rev. Sci. Instrum. 79 (2008) 074501.
- [17] F. Acerne, G. Giordano, R. Romano, R. De Rosa, F. Barone, Tunable mechanical monolithic sensor with interferometric readout for low frequency seismic noise measurement, Nucl. Instrum. Methods Phys. Res. A 617 (2010) 457–458.
- [18] F. Acerne, G. Giordano, R. Romano, F. Barone, Compact tunable monolithic sensors for vibration monitoring and control of structures and very low frequency large band characterization of sites, in: 15th World Conference in Earthquake Engineering, 24–28 September 2012, Lisbon, Portugal, 2012.
- [19] D. Gardner, T. Hofler, S. Baker, R. Yarber, S. Garrett, A fiber-optic interferometric seismometer, J. Lightwave Technol. 5 (7) (July 1987) 953–960.
- [20] A. Araya, K. Kawabe, T. Sato, M. Mio, K. Tsubono, Highly sensitive wideband seismometer using a laser interferometer, Rev. Sci. Instrum. 64 (5) (1993) 1337–1341.
- [21] A. Araya, K. Sekiya, Y. Shindo, Broadband seismometer for ocean bore-hole observations, in: Symposium on Underwater Technology and Workshop on Scientific Use of Submarine Cables and Related Technologies, 2007, pp. 245–248.

- [22] I. Littler, J. Chow, D. Mclelland, A system, device and method for detecting seismic acceleration, WO2010057247, 2010.
- [23] D. Chatrefou, Fiber-optic vibration sensor, EP354882, 2003.
- [24] B. Levine, Simple fiber optic seismometer for harsh environments, US7714271, 2007.
- [25] B. Levine, Fiber optic microseismic sensing systems, WO201150275, 2011.
- [26] R. Cahill, E. Udd, Optical vibration sensor, US4471659, 1984.
- [27] B. Merchant, M. Okandan, An Interferometric MEMS Seismometer: Design and Testing, 2009, pp. 352.
- [28] P.R. Saulson, Thermal noise in mechanical experiments, Phys. Rev. D 42 (8) (1990) 2437–2445.
- [29] M.J. Downs, K.W. Raine, An unmodulated bi-directional fringe-counting interferometer system for measuring displacement, Appl. Mech. Mater. 365 (1979) 85–88.
- [30] J. Hrabina, J. Lazar, M. Hola, O. Cip, Frequency noise properties of lasers for interferometry in nanometrology, Sensors 13 (2) (2013) 2206–2219.
- [31] M. Zumberge, J. Berger, M. Dzieciuch, R. Parker, Resolving quadrature fringes in real time, Rev. Sci. Instrum. 43 (4) (2004) 771–775.
- [32] D. Ponceau, P. Millier, S. Olivier, Subnanometric Michelson Interferometry for Seismological Applications, 2008, pp. 70030.
- [33] M. Zumberge, M. Berger, R. Parker, Resolving quadrature fringes in real time, US patent 8023116B1, 2011.

Biographies



Christophe Collette received M.Sc. and Ph.D. degrees in mechanical engineering from the Université Libre de Bruxelles in 2003 and 2007. Since 2014, he is professor in the Faculty of Engineering at the ULB and is member of the BEAMS department. His main research interests include the precision and vibration control of large instruments dedicated to experimental physics.



Fares Nassif received M.S. in Mechatronics and Mechanical Construction form Universite Libre de Bruxelles (ULB) in 2012 and 2014 respectively. His master was focused on measuring ground vibrations at low frequencies. A sensor immune to tilt-to-horizontal coupling was studied and presented. Also a sensor fusion experiment between an inertial sensor and a seismometer in order to increase sensing bandwidth was undertaken.



Julien Amar recently received his engineering degree from the Université de Technologie de Belfort Montbéliard (UTBM) in 2015 in France by doing several research projects, such as the realization of an optical inertial sensor at the University libre de Bruxelles and the conception of a C++ autonomous program for a parrot AR.Drone using OpenCV at Wakayama university, Japan.



Céline Depouhon received her M.S. in Mechatronics and Mechanical Construction from Universite Libre de Bruxelles in 2014. Her master thesis was focused on swarm robotics and more specially the distributed control of multi-robot systems. Her research interests include also optical inertial sensor and Michelson interferometer.



Simon-Pierre Gorza received his M.S. and Ph.D. degrees in physical engineering from the Université libre de Bruxelles (ULB) in 2001 and 2005, respectively. Since 2010 he is professor in the Faculty of Engineering at the ULB and is a member of the OPERA-photonic group. His main research interests include spatial and temporal dynamics in optical nonlinear media, pulse characterization techniques and application of linear and nonlinear optics to bio-imaging and sensors.